Korean J. Chem. Eng., 36(6), 843-850 (2019)
DOI: 10.1007/s11814-019-0269-z

pISSN: 0256-1115
eISSN: 1975-7220

Characteristics of exfoliated HNb_3O_8 nanosheet derived from amorphous niobic acid and its application to dehydration of 2-heptanol

Jongha Park* and Young-Woong Suh*,,†**

*Department of Chemical Engineering, Hanyang University, Seoul 04763, Korea
**Research Institute of Industrial Science, Hanyang University, Seoul 04763, Korea
(*Received 8 January 2019 • accepted 8 April 2019*)

Abstract−The synthesis of exfoliated HNb_3O_8 nanosheet ($eHNb_3O_8$) generally starts from the mixing of K_2CO_3 with crystalline Nb_2O_5 and involves a very routine procedure in subsequent multi-steps. Herein, we report for the first time the use of niobic acid (NBA, $Nb_2O_5{\cdot}nH_2O$) as Nb source for the preparation of final $eHNb_3O_8$. Different from the analogue derived from crystalline Nb_2O_5, the prepared nanosheet contains a very small amount of potassium ion and exhibits high stability in consecutive runs for the dehydration reaction. The linkage between these two features is confirmed by the inferior stability of potassium-deficient $eHNb_3O_8$ samples prepared via prolonged proton-exchange. When a series of niobate materials are examined, the remarkable finding is the higher K/Nb ratio in NBA-derived KNb_3O_8 than the theoretical value. This is attributed to the acidity of amorphous NBA by which the carbonate ion of K_2CO_3 is decomposed into CO_2 in the preparation of the solid mixture K_2CO_3-NBA. These more intercalated K^+ cannot be all displaced with proton by the general ion-exchange process employed for Nb_2O_5-derived $eHNb_3O_8$. Consequently, the proposed model suggests that the potassium ion remaining in NBA-derived $eHNb_3O_8$ acts as a ligating element to tie up a single, exfoliated nanosheet into several.

Keywords: Exfoliated HNb_3O_8 Nanosheet, Amorphous Niobic Acid, Potassium Ion

INTRODUCTION

A variety of layered metal oxides, including HNb_3O_8, $HTiNbO_5$, HTi_2NbO_7, $HSr_2Nb_3O_{10}$, $HNbWO_6$, $HNbMoO_6$, and $HTaWO_6$, have been transformed into the corresponding exfoliated nanosheet materials in order to make easy access of a substrate into catalytically active sites. Owing to unique nanosheet structure, exfoliated HNb_3O_8 ($eHNb_3O_8$) was reported to be powerful in various applications including acid-catalyzed reactions [1-3], and photocatalytic reactions [4,5]. Furthermore, $eHNb_3O_8$ was used as a support for Pd loading and the resulting bifunctional catalyst showed the great performance in cascade reactions [6].

The synthesis of $eHNb_3O_8$ followed a very routine procedure in multi steps such as solid-state mixing, thermal treatment for the formation of layered KNb_3O_8, potassium exchange with proton to yield a layered HNb_3O_8, and finally exfoliation/aggregation [7-9]. This procedure has been rarely modified so far because it was effective in producing the nanosheet of a single atomic layer. Even though this is understood more or less, the synthesis detail on one or more of the aforementioned involved steps needs to be modified since the whole process is much too time consuming. We recently demonstrated the improved exfoliation efficiency and recovery of $eHNb_3O_8$ by effective contact between Nb_2O_5 and K_2CO_3 [10]. For this purpose we contacted crystalline Nb_2O_5 with an aqueous K_2CO_3 solution prior to ball-milling, called "liquid-state mixing" to distinguish from the conventional solid-state mixing to use solid K_2CO_3. It led to the formation of homogeneous K_2CO_3-Nb_2O_5 mixture and the intercalation of a little more potassium ion in the layered KNb_3O_8. These positive effects resulted from facile diffusion of K^+ into the crystalline lattice of Nb_2O_5 by the liquid-state mixing. This suggests that the efficiency in the exfoliation step would be determined by how to achieve a high degree of such diffusion in the first mixing step because high crystallinity of Nb_2O_5 functions as an obstacle.

In this respect, niobic acid ($Nb_2O_5{\cdot}nH_2O$) needs to be considered an appropriate starting material instead of crystalline Nb_2O_5. Since it is indeed amorphous and contains a large variety of hydroxyl groups [11,12], the diffusion of K^+ in the mixing step is expected to proceed at a fast rate. Nevertheless, it is hard to assure whether this will bring about a positive effect on the activity and stability of final $eHNb_3O_8$ derived from niobic acid. Thus, niobic acid was herein used as Nb source for producing $eHNb_3O_8$. Because there have been no associated reports so far, the liquid-state mixing we applied for crystalline Nb_2O_5 was used in this work as it is. The assessment started from comparing the niobate structures obtained in a series of preparation steps, KNb_3O_8-*x*, HNb_3O_8-*x* and $eHNb_3O_8$-*x*, where *x* is A or C for amorphous $Nb_2O_5{\cdot}nH_2O$ or crystalline Nb_2O_5, respectively. Several characterization works revealed that more K^+ remains in $eHNb_3O_8$-A and even in HNb_3O_8-A. To tune the content of K^+ present in $eHNb_3O_8$-A, additional treatments were conducted. The prepared $eHNb_3O_8$ samples were tested in the dehydration of 2-heptanol as a model reaction and their stability was evaluated in three consecutive activity runs. Consequently, an explanation was formulated for the characteristics of a series of

†To whom correspondence should be addressed.
E-mail: ywsuh@hanyang.ac.kr

Table 1. Summary of $eHNb_3O_8$ samples prepared by the liquid-state mixing method

Sample code[a]	Nb source	Ion-exchange period in Step 3	HCl ion-exchange in Step 4	K/Nb ratio in KNb_3O_8 samples
$eHNb_3O_8$-C	Nb_2O_5	72 h	X	0.32
$eHNb_3O_8$-A	$Nb_2O_5{\cdot}nH_2O$	72 h	X	0.47
$eHNb_3O_8$-A1	$Nb_2O_5{\cdot}nH_2O$	120 h	X	0.30
$eHNb_3O_8$-A2	$Nb_2O_5{\cdot}nH_2O$	72 h	O (72 h)	0.32

[a]C and A stand for crystalline Nb_2O_5 and amorphous $Nb_2O_5{\cdot}nH_2O$, respectively

niobate structures derived from niobic acid.

EXPERIMENTAL

1. Catalyst Preparation

Exfoliated nanosheet samples listed in Table 1 were prepared via the following four steps.

Step 1, liquid-state mixing: A solid Nb source of 0.029 mol Nb, crystalline Nb_2O_5 (Junsei Chemical Co., Ltd.) or niobic acid $Nb_2O_5{\cdot}nH_2O$ (HY-340 provided by CBMM in Brazil) was mixed with an aqueous K_2CO_3 solution (0.01 mol, 400 mL) for 30 min. Then, the suspension was dried in a convection oven at 373 K overnight.

Step 2, ball-milling and calcination: The obtained solid mixture (ca. 7.8 g) was placed in a polypropylene bottle of 100 cm^3 with ten Zr balls of 10 mm diameter. The bottle was horizontally rotated at a speed of 200 rpm at room temperature for 24 h. The ball-milled material was calcined at 1,373 K for 5 h (ramping rate: 5 K min^{-1}).

Step 3, proton exchange: The calcined material KNb_3O_8 was ion-exchanged with 60 wt% HNO_3 solution (150 mL) for 72 h at room temperature, followed by washing with distilled water three times and drying at 373 K overnight. For the sample $eHNb_3O_8$-A1, ion-exchange was performed for 120 h.

Step 4, exfoliation and aggregation: The resulting H^+-exchanged niobate (HNb_3O_8) was added to 2.5 wt% tetrabutylammonium hydroxide (TBAOH; used after dilution of 40 wt% solution purchased from Sigma-Aldrich Co.) solution of 200 mL and stirred for 72 h under ambient condition, followed by the addition of an aqueous HNO_3 solution (60 wt%, 100 mL) to recover the exfoliated HNb_3O_8 nanosheet as aggregates. The white $eHNb_3O_8$ sample was collected by vacuum filtration, washed with distilled water and finally dried at 375 K for 24 h. This dry $eHNb_3O_8$ was ground and sieved to less than 200 μm. For the sample $eHNb_3O_8$-A2, additional ion-exchange with a 60 wt% HCl solution was conducted for 72 h.

The conventional solid-state mixing method was also employed. The aforementioned procedure was used in the same manner except the mixing step that the physical mixture of K_2CO_3 (0.01 mol) and Nb source (Nb of 0.029 mol) was ground using a mortar and pestle, and then ball-milled at a speed of 200 rpm at room temperature for 72 h.

2. Characterization

The Brunauer-Emmett-Teller (BET) surface area (ca. 0.2 g sample) was measured at 77 K using a Micromeritics 3-Flex after pretreatment at 423 K for 1 h under vacuum. Powder X-ray diffraction (XRD) analysis was performed with a Rigaku MiniFlex 600 using a Cu Kα radiation source with 40 kV and 30 mA. Thermogravimetric analysis coupled with an MS detector (TGA-MS) was conducted in a NETZSCH TG209F1/QMS403C as the sample (ca. 10 mg) was heated to 1,173 K at a rate of 5 K min^{-1} in an air flow (100 ml min^{-1}). Also, TG analysis was used to calculate the number of water molecules in amorphous niobic acid. Transmission electron microscope with an energy-dispersive X-ray spectrometer (TEM-EDS) was operated with a JEOL JEM-2100F at a voltage of 200 kV. Pyridine-chemisorbed FT-IR experiments were carried out in a Thermo Nicolet 6700 spectrometer equipped with an MCT-A detector. The pelletized sample (30 mg, 0.65 cm radius) installed in a Specac HTHP cell was pretreated at 523 K for 3 h under vacuum and cooled to 423 K. After pyridine (0.5 μL) was injected to the chamber, the sample was exposed for 30 min and evacuated for 30 min before pyridine-chemisorbed FT-IR spectrum was acquired (Figs. S1-S3).

3. Activity Test in the Dehydration of 2-Heptanol

Exfoliated nanosheet samples were tested in the dehydration of 2-heptanol using a stainless-steel batch reactor (100 cm^3) into which the catalyst (0.1 g) and 2-heptanol (0.086 mol) were charged. The as-prepared catalyst samples were used without treatment or were pretreated at 523 K in a N_2 flow prior to the activity test. After the reactor inside was purged with N_2 for more than 3 h, the reaction was conducted at 513 K for 6 h under N_2, where the autogenous pressure approached 30 barg. After cooling to ambient temperature, the product mixture was taken out, filtered through a syringe filter (0.45 μm diameter) and mixed with an internal standard of acetone. An aliquot of this sample was analyzed in a gas chromatograph (Younglin YL6100) equipped with an FID detector and an HP-Innowax column (50 m, 0.2 mm, 0.4 μm). The conversion of 2-heptanol was calculated by dividing the mole of 2-heptanol consumed by the initial mole of 2-heptanol.

For consecutive activity runs, the catalyst sample was separated from the product mixture by vacuum filtration. The collected sample was washed with acetone three times and then cleaned with distilled water. The sample was dried at 333 K before the next reaction started.

RESULTS AND DISCUSSION

1. Niobate Structures Derived from Amorphous $Nb_2O_5{\cdot}nH_2O$ and Crystalline Nb_2O_5

Since amorphous niobic acid $Nb_2O_5{\cdot}nH_2O$ (hereafter abbreviated as NBA) has never been utilized for the preparation of $eHNb_3O_8$, we attempted to characterize the samples obtained in each of the preparation steps by XRD. When the ball-milled mixture of NBA and K_2CO_3 was first accessed, no reflections were observed (Fig.

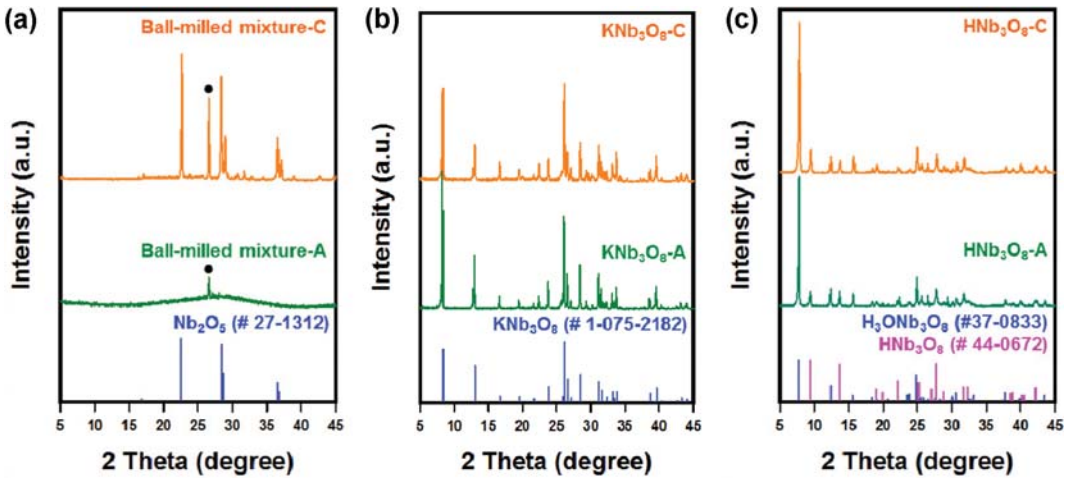

Fig. 1. XRD patterns of niobate structures derived from NBA (designated as -A) crystalline Nb_2O_5 (designated as -C). (a) Ball-milled mixtures. (b) Calcined KNb_3O_8 samples. (c) Proton exchanged HNb_3O_8 samples. The black circle in (a) represents the reflection of graphite that is an internal standard.

1(a)). This is simply because NBA is amorphous and the particle size of K_2CO_3 decreases below an XRD detectable limit. The latter is supported by the XRD pattern of the ball-milled mixture of crystalline Nb_2O_5 and K_2CO_3 in which all reflections correspond to Nb_2O_5 of T phase (PDF #27-1312). Therefore, it can be presumed that the potassium ion is spread well on the surface of NBA.

This assumption was verified by the XRD pattern of KNb_3O_8-A obtained after calcination at 1,373 K. As shown in Fig. 1(b), the reflections of KNb_3O_8-A matched well with the standard reflections of KNb_3O_8 (PDF #1-075-2182). Also, they were similar to the reflections of KNb_3O_8-C, meaning that the layered KNb_3O_8 structure is developed by calcination of the mixture K_2CO_3-NBA at a similar level to that derived from the mixture K_2CO_3-Nb_2O_5. Note that the peak intensity at 2θ of 33.68° corresponding to the (080) plane of KNb_3O_8 can vary depending on the packing intensity of the prepared XRD specimens. A similarity was also found in the XRD patterns of HNb_3O_8-A and HNb_3O_8-C obtained after proton exchange with HNO_3 (Fig. 1(c)). The two samples exhibited the reflections at the 2θ of 7.87° and 9.70° corresponding to the (020) plane of $H_3ONb_3O_8$ (PDF #44-0672) and HNb_3O_8 (PDF #37-0833), respectively. Each of these structures is generally determined by the presence or absence of H_2O molecules intercalated within niobate interlayers [9]. Therefore, XRD results suggest that when NBA is used as a starting material, steps such as KNb_3O_8 formation and proton exchange proceed analogously to the case of using crystalline Nb_2O_5.

XRD patterns of the exfoliated nanosheet samples were finally examined. They did not appear to have distinct reflections at the intensity scale identical to that of the aforementioned samples (Fig. 2), due to the thickness of several atomic layers. However, when the patterns of $eHNb_3O_8$-A and $eHNb_3O_8$-C were blown up with a magnification of ten, more intense reflections were observed for $eHNb_3O_8$-A compared to $eHNb_3O_8$-C and matched with those of $K_3Nb_7O_{19}$ (PDF #38-1499) [13]. This suggests that a very small amount of potassium ion still remains in the structure of $eHNb_3O_8$-A derived from NBA, different from $eHNb_3O_8$-C, although the

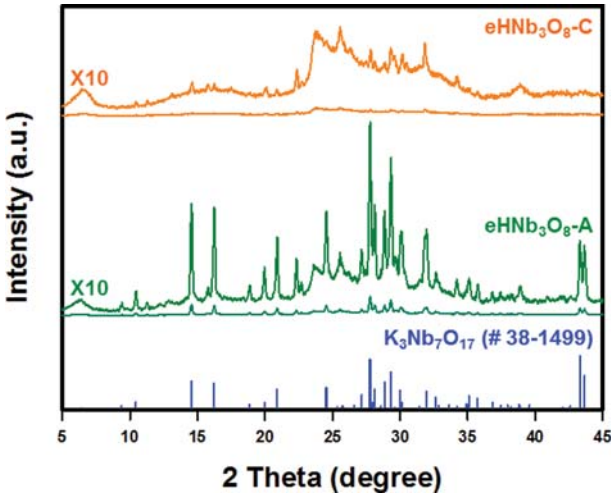

Fig. 2. XRD patterns of exfoliated nanosheet samples $eHNb_3O_8$-A and $eHNb_3O_8$-C.

identical procedure in all preparation steps was applied for both samples.

The activity test was then performed using the prepared exfoliated nanosheet samples because we could hardly forecast how much the potassium ion remaining in $eHNb_3O_8$-A affects the activity and stability in the dehydration reaction. The as-prepared samples $eHNb_3O_8$-A and $eHNb_3O_8$-C were tested in the dehydration of 2-heptanol at 513 K for 6 h under N_2. In the first run, the fresh $eHNb_3O_8$-C was superior by ca. 15% to fresh $eHNb_3O_8$-A (Fig. 3(a)). However, the consecutive runs revealed that the conversion of 2-heptanol decreased to 72.1% for $eHNb_3O_8$-C whereas it was maintained around 80% for $eHNb_3O_8$-A. To understand these activity results, the per-gram-based amount of Brønsted acid sites (BAS) was measured by pyridine-chemisorbed FT-IR experiments for fresh samples as well as spent samples after the first and second reaction runs (Fig. 3(b)). For fresh samples, the amount of BAS was higher in $eHNb_3O_8$-C (8.5 μmol g^{-1}) than in $eHNb_3O_8$-

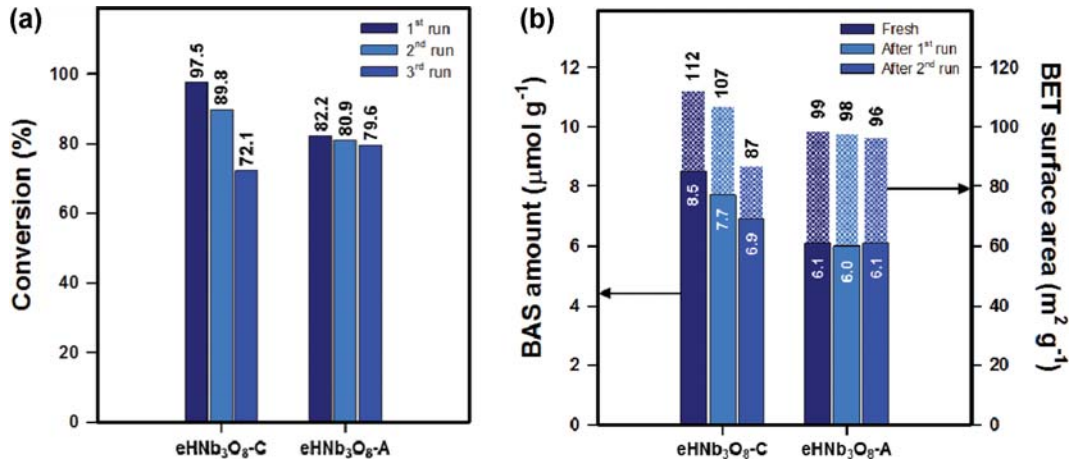

Fig. 3. Activity of the as-prepared $eHNb_3O_8$-A and eNb_3O_8-C samples in the dehydration of 2-heptanol for consecutive runs. (a) Conversion of 2-heptanol. (b) BAS amount and BET surface area.

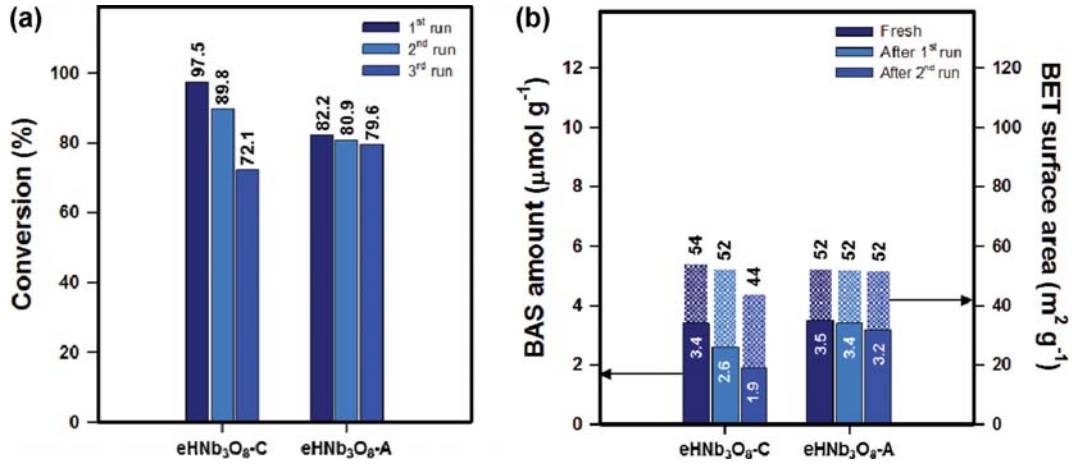

Fig. 4. Activity of the 523 K-pretreated $eHNb_3O_8$-A and eNb_3O_8-C samples in the dehydration of 2-heptanol for consecutive runs. (a) Conversion of 2-heptanol. (b) BAS amount and BET surface area.

A (6.1 μmol g^{-1}), which explains the better activity of fresh $eHNb_3O_8$-C. Moreover, the BAS amount of $eHNb_3O_8$-C decreased as it was repeatedly used, but such a decrease was not found in $eHNb_3O_8$-A. These acidity results are consistent with what we obtained in consecutive activity runs. Nevertheless, the inferior stability of $eHNb_3O_8$-C compared to $eHNb_3O_8$-A was an unexpected finding.

Thus, additional activity tests were conducted after the as-prepared catalyst samples were subjected to thermal pretreatment at 523 K because their structures may be changed at the reaction temperature of 513 K. Note that such pretreatment caused the sintering of exfoliated nanosheets resulting in the decrease in the BAS amount (cf. Figs. 3(b) and 4(b)). It was observed once again that $eHNb_3O_8$-A experienced a negligible activity loss, whereas the activity of $eHNb_3O_8$-C in the third run dropped to 67% of the initial activity (Fig. 4(a)). Similarly, a significant loss in the BAS amount was observed in $eHNb_3O_8$-C but not in $eHNb_3O_8$-A (Fig. 4(b)).

Additionally, the BET surface area of the fresh and spent catalyst samples was measured. Figs. 3(b) and 4(b) clearly show that the BET surface area of $eHNb_3O_8$-C decreased as the reaction run was repeated, whereas that of $eHNb_3O_8$-A was changed negligibly in the consecutive runs, as found in the BAS amount. When the conversion of 2-heptanol was plotted against the BAS amount and BET surface area of all fresh and spent catalyst samples tested in this work, the activity was observed to be in a linear relationship with the two catalyst properties, depending on the sample pretreatment condition (Fig. S4). This suggests that both the BAS amount and BET surface area affect the catalytic activity of $eHNb_3O_8$ samples.

2. Removal of Potassium ion in HNb_3O_8-A and $eHNb_3O_8$-A

From the above results, it was presumed that the potassium ion remaining in $eHNb_3O_8$-A influences the activity and stability in the reaction. Thus, we examined the presence of potassium ion in the layered HNb_3O_8-A by TEM-EDS. As presented in Fig. 5(a), there was no potassium detected in the K mapping image of HNb_3O_8-C. However, some local spots were seen in the corresponding image of HNb_3O_8-A, where the atomic percentage of K was 0.11%. Additionally, layered KNb_3O_8 samples were characterized by TEM-EDS (Fig. 5(b)). The densities of K and Nb elements were higher for KNb_3O_8-C due to thick particles. The interesting finding was the

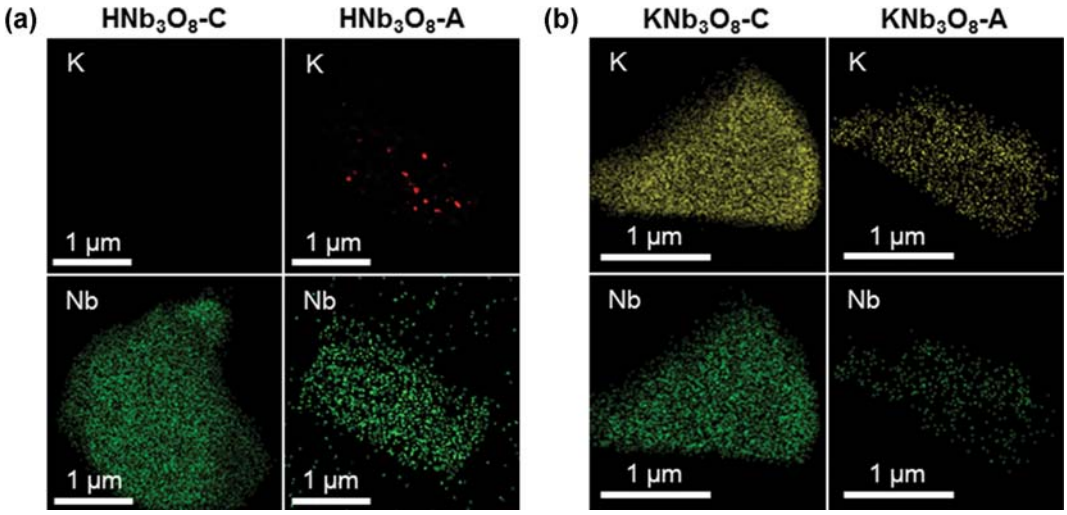

Fig. 5. K and Nb EDS mapping images of layered niobate samples. (a) HNb_3O_8-C and HNb_3O_8-A. (b) KNb_3O_8-C and KNb_3O_8-A.

different atomic K/Nb ratios in KNb_3O_8-C (0.32) and KNb_3O_8-A (0.47). Since the theoretical K/Nb ratio is 0.33, the higher value of KNb_3O_8-A indicates that potassium ions are more intercalated into the structure of KNb_3O_8 derived from NBA.

For confirmation, conventional solid-state mixing was employed for preparing the layered KNb_3O_8-A and HNb_3O_8-A samples. In their TEM-EDS images, the atomic percentage of K in HNb_3O_8-A was estimated to be 0.12% (Fig. S5) and the atomic K/Nb ratio was 0.52 (Fig. S6). Consequently, the standard ion-exchange period of three days with an HNO_3 solution is not enough to displace all potassium ions present in KNb_3O_8-A by protons because more intercalated potassium ions are present in this sample compared to KNb_3O_8-C. This is an unexpected result that originates from the use of NBA.

Thus, two control $eHNb_3O_8$ samples were prepared. First, KNb_3O_8-A was ion-exchanged with a 60 wt% HNO_3 solution for 120 h (longer than the standard period). The so-obtained HNb_3O_8 was exfoliated and aggregated in an identical manner to $eHNb_3O_8$-A,

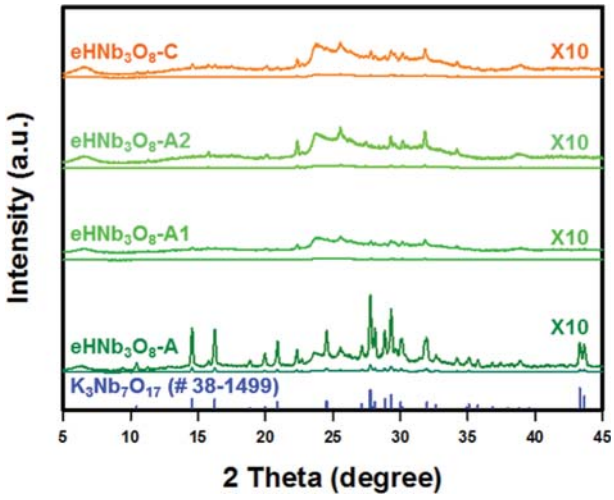

Fig. 6. Blown-up XRD patterns of $eHNb_3O_8$-A1 and $eHNb_3O_8$-A2 compared to $eHNb_3O_8$-A (bottom) and $eHNb_3O_8$-C (top).

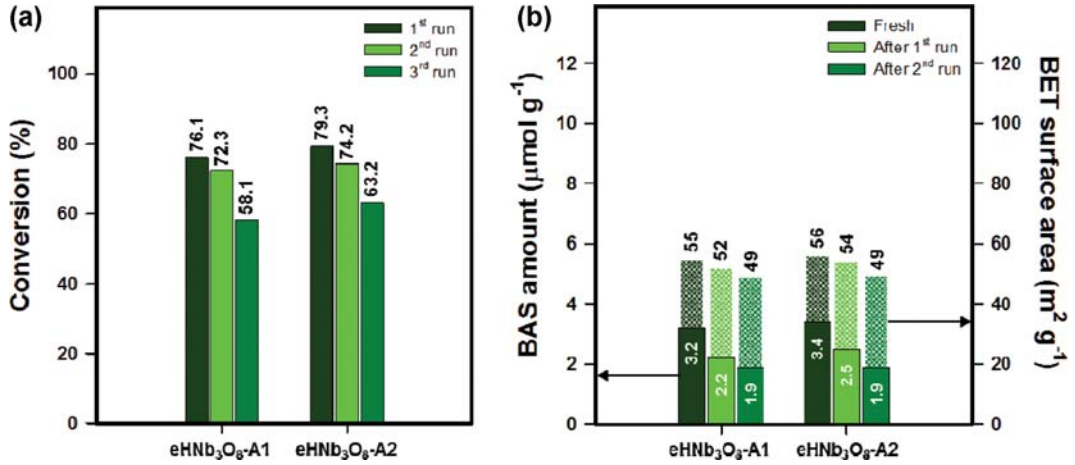

Fig. 7. Activity of the 523 K-pretreated $eHNb_3O_8$-A1 and eNb_3O_8-A2 samples in the dehydration of 2-heptanol for consecutive runs. (a) Conversion of 2-heptanol. (b) BAS amount and BET surface area.

producing the sample $eHNb_3O_8$-A1. Second, $eHNb_3O_8$-A was ion-exchanged again with a 60 wt% HCl solution, resulting in the sample $eHNb_3O_8$-A2. The XRD patterns of these control samples show the negligible reflections of $K_3Nb_7O_{19}$ like $eHNb_3O_8$-C (Fig. 6). This means that ion-exchange needs to be conducted deliberately when $eHNb_3O_8$ is derived from NBA.

The dehydration activity and stability of these two control samples were examined after thermal treatment at 523 K. Surprisingly, the conversion of 2-heptanol in three consecutive runs decreased from 76.1% to 58.1% for $eHNb_3O_8$-A1 and from 79.3% to 63.2% for $eHNb_3O_8$-A2 (Fig. 7(a)). Although these conversion values are different from those obtained with $eHNb_3O_8$-C, the activity declines were very similar to one another. The BAS amount also decreased as $eHNb_3O_8$-A1 and $eHNb_3O_8$-A2 were used repeatedly (Fig. 7(b)). Therefore, it is believed that the catalyst stability of $eHNb_3O_8$-A is associated with the potassium ion remaining in its nanosheet structure.

3. Tracing the Origin of the Potassium Ion Present in $eHNb_3O_8$

The higher K/Nb ratio in KNb_3O_8-A explains the diffusion of more potassium ion into NBA in the ball-milling step. Thus, the thermal decomposition behavior of K_2CO_3-Nb_2O_5 and K_2CO_3-NBA mixtures obtained after ball-milling was investigated by TGA-MS analysis. The weight loss at 1,173 K was measured to be similar at ca. 12.0% for both mixtures (Fig. 8(a)). However, the derivatives of TG curves were different from each other, along with the mass fragments of m/z=18 and 44 corresponding to H_2O and CO_2, respectively (Fig. 8(b)). The mixture K_2CO_3-Nb_2O_5 showed two decomposition peaks in the ranges 300-450 and 700-900 K of which

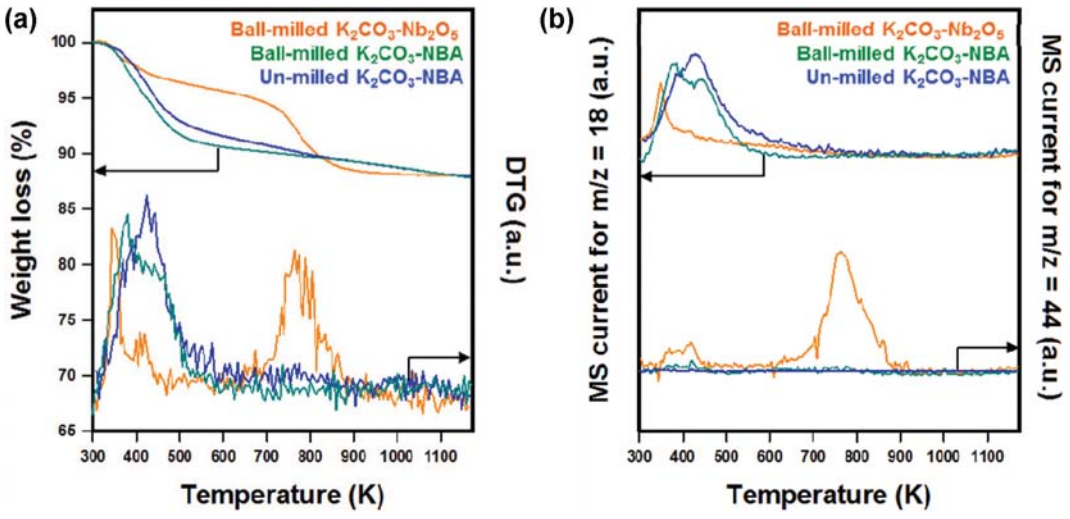

Fig. 8. Thermal decomposition of ball-milled K_2CO_3-NBA (green), ball-milled K_2CO_3-Nb_2O_5 (orange) and un-milled K_2CO_3-NBA (blue) mixtures. (a) TG curves and their derivative (DTG) curves. (b) MS currents for m/z=18 and 44 corresponding to H_2O and CO_2, respectively.

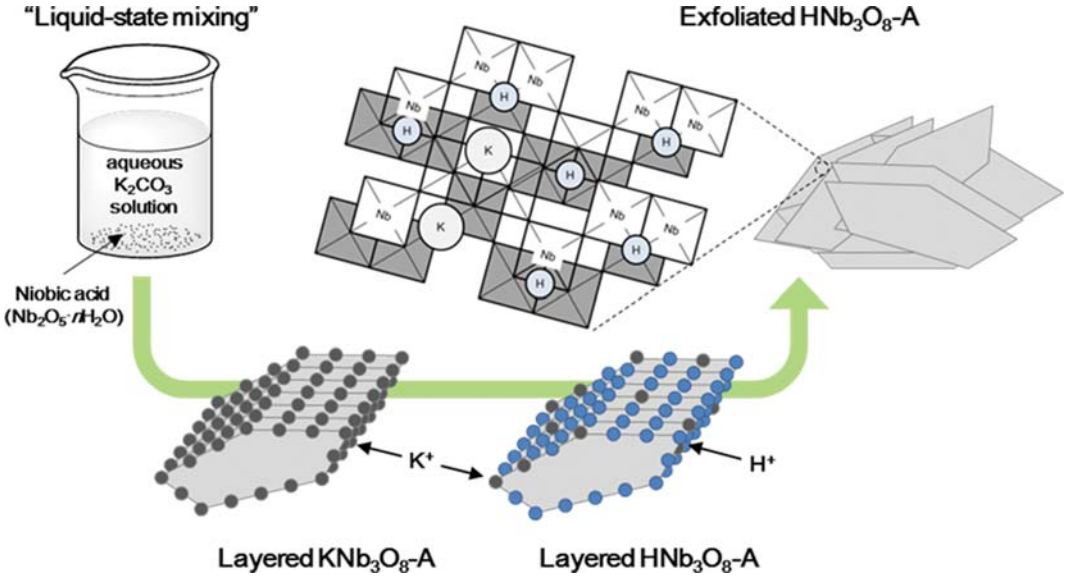

Fig. 9. Schematic for the preparation of $eHNb_3O_8$-A.

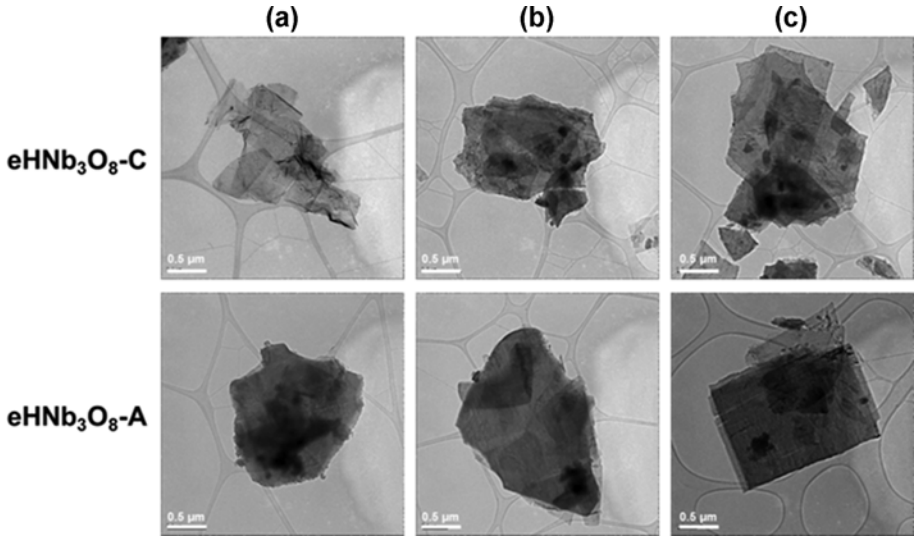

Fig. 10. TEM images of the 523 K-pretreated $eHNb_3O_8$-A (bottom) and $eHNb_3O_8$-C (top). (a) Fresh samples. (b) Spent samples after the first activity run. c Spent samples after the third activity run.

each mainly represents the emission of H_2O and CO_2, respectively. In contrast, a single, broad peak in the range 300-600 K was observed in the decomposition of the mixture K_2CO_3-NBA. As clearly seen in Fig. 8(b), this peak is ascribed to the emission of water because of H_2O molecules existing in NBA ($Nb_2O_5 \cdot nH_2O$). The remarkable finding to note is no emission of CO_2 from the mixture K_2CO_3-NBA, which is different from the mixture K_2CO_3-Nb_2O_5 showing CO_2 emission in 700-900 K [10,14]. While searching for a possible reason about no CO_2 emission in the former mixture, we found that gas bubbles were generated in an aqueous K_2CO_3 solution containing NBA (Fig. S7). Thus, the dry, un-milled K_2CO_3-NBA mixture was characterized by TGA-MS analysis. As shown in Fig. 8(b), CO_2 emission was not observed, meaning that the carbonate ion was totally decomposed into CO_2 in the step of liquid-state mixing. This is possibly due to acid-catalyzed carbonate decomposition by the high acidity of NBA, which generally happens in acidic media.

4. Proposed Model for the Preparation of $eHNb_3O_8$-A

Based upon the characterization results about a series of niobate structures derived from NBA, the model can be proposed to explain the better stability of $eHNb_3O_8$-A compared to $eHNb_3O_8$-C (Fig. 9). When crystalline Nb_2O_5 is used, the potassium and carbonate ions diffuse competitively into the lattice of Nb_2O_5 in the ball-milling step, followed by high-temperature calcination to result in the K^+-intercalated niobate material close to the theoretical K/Nb ratio of KNb_3O_8. However, the carbonate ion would be liberated into CO_2 upon contact of NBA with a K_2CO_3 solution. Thus, the potassium ion solely infiltrates into the NBA structure, leading to the over-presence of K relative to Nb in KNb_3O_8-A. The standard ion-exchange process applied for KNb_3O_8-C is, therefore, not enough to fully displace the potassium ion of KNb_3O_8-A by the proton; thus, prolonged exposure to a concentrated HNO_3 solution is required for complete ion-exchange, as revealed in the XRD pattern of $eHNb_3O_8$-A1. Since KNb_3O_8-A is subjected to the identical ion-exchange process to KNb_3O_8-C, a very small amount of potassium ion exists in the niobate interlayers of HNb_3O_8-A and even in $eHNb_3O_8$-A. In contrast, the potassium ion is absent in the molecular structure of $eHNb_3O_8$-C due to the complete ion-exchange of KNb_3O_8-C.

As examined in the activity results over $eHNb_3O_8$-A1 and $eHNb_3O_8$-A2, the remaining potassium ion is responsible for the better stability of $eHNb_3O_8$-A. Thus, TEM images of fresh and spent catalyst samples were taken. For fresh samples, the nanosheet of $eHNb_3O_8$-C looks much thin compared to that of $eHNb_3O_8$-A (Fig. 10). However, the TEM image of $eHNb_3O_8$-C recovered after the third activity run shows the stacking of exfoliated nanosheets, whereas no significant difference was found between TEM images of fresh and recovered $eHNb_3O_8$-A. Therefore, it can be suggested that the potassium ion acts as a ligating element to tie up a single, exfoliated nanosheet into several.

CONCLUSION

Amorphous NBA was used for the first time as Nb source to produce the exfoliated HNb_3O_8 material. Due to the acidity of NBA, KNb_3O_8 obtained after ball-milling and calcination showed higher K/Nb ratio than the analogue prepared using crystalline Nb_2O_5. Hence, the ion-exchange process employed for Nb_2O_5-derived KNb_3O_8 could not remove the potassium ion perfectly, resulting in a very small amount of the potassium ion being present in the layered HNb_3O_8 and moreover in the final $eHNb_3O_8$. The remaining potassium ion was believed to play a role in ligating the single nanosheet into several, which was supported by the better stability of NBA-derived $eHNb_3O_8$ in consecutive reactions runs as well as TEM images of spent catalysts. The proposed model explained that all results examined in a series of niobate structures originated from the use of NBA. Therefore, this report opens the potential of amorphous niobic acid in the preparation of exfoliated Nb-containing nanosheet materials and also implies the importance of ligating elements (herein, the potassium ion) affecting their stability.

ACKNOWLEDGEMENTS

This work was supported by the Korea Institute of Energy Technology Evaluation and Planning under the Ministry of Trade, Industry and Energy, Republic of Korea (KETEP-20142010201800 and KETEP-20163010092210), as well as by the Basic Science Research Program through the National Research Foundation of Korea under the Ministry of Education, Republic of Korea (NRF-2016R1A6A1A03013422).

SUPPORTING INFORMATION

Additional information as noted in the text. This information is available via the Internet at http://www.springer.com/chemistry/journal/11814.

REFERENCES

1. A. Takagaki, D. Lu, J. N. Kondo, M. Hara, S. Hayashi and K. Domen, *Chem. Mater.*, **17**, 2487 (2005).
2. A. Takagaki, C. Tagusagawa, S. Hayashi, M. Hara and K. Domen, *Energy Environ. Sci.*, **3**, 82 (2010).
3. Z. J. Yang, L. F. Li, Q. B. Wu, N. Ren, Y. H. Zhang, Z. P. Liu and Y. Tang, *J. Catal.*, **280**, 247 (2011).
4. J. Xiong, Y. Liu, S. Liang, S. Zhang, Y. Li and L. Wu, *J. Catal.*, **342**, 98 (2011).
5. J. Xiong, L. Wen, F. Jiang, Y. Liu, S. Liang and L. Wu, *J. Mater. Chem. A*, **3**, 20627 (2015).
6. N. Lee and Y.-M Chung, *Appl. Surf. Sci.*, **370**, 160 (2016).
7. K. Nassau, J. W. Shiever and J. L. Bernstein, *J. Electrochem. Soc.*, **116**, 348 (1969).
8. P. M. Gasperin, *Acta Crystallogr.*, **B38**, 2024 (1982).
9. R. Nedjar, M. M. Borel and B. Raveau, *Mater. Res. Bull.*, **20**, 1291 (1985).
10. J. Park, J.-H. Lee, Y.-M. Chung and Y.-W. Suh, *Adv. Powder Technol.*, **28**, 2524 (2017).
11. B. K. Sen, A. V. Saha and N. Chatterjee, *Mater. Res. Bull.*, **16**, 923 (1981).
12. T. Ikeya and M. Sennna, *J. Non-Cryst. Solids*, **105**, 243 (1988).
13. G. D. Fallon, B. M. Gatechous and L. Guddat, *J. Solid State Chem.*, **61**, 181 (1986).
14. T. Rojac, M. Kosec, P. Šegedin, B. Malič and J. Holc, *Solid State Ionics*, **177**, 2987 (2006).

Supporting Information

Characteristics of exfoliated HNb_3O_8 nanosheet derived from amorphous niobic acid and its application to dehydration of 2-heptanol

Jongha Park* and Young-Woong Suh*,,†**

*Department of Chemical Engineering, Hanyang University, Seoul 04763, Korea
**Research Institute of Industrial Science, Hanyang University, Seoul 04763, Korea
(*Received 8 January 2019 • accepted 8 April 2019*)

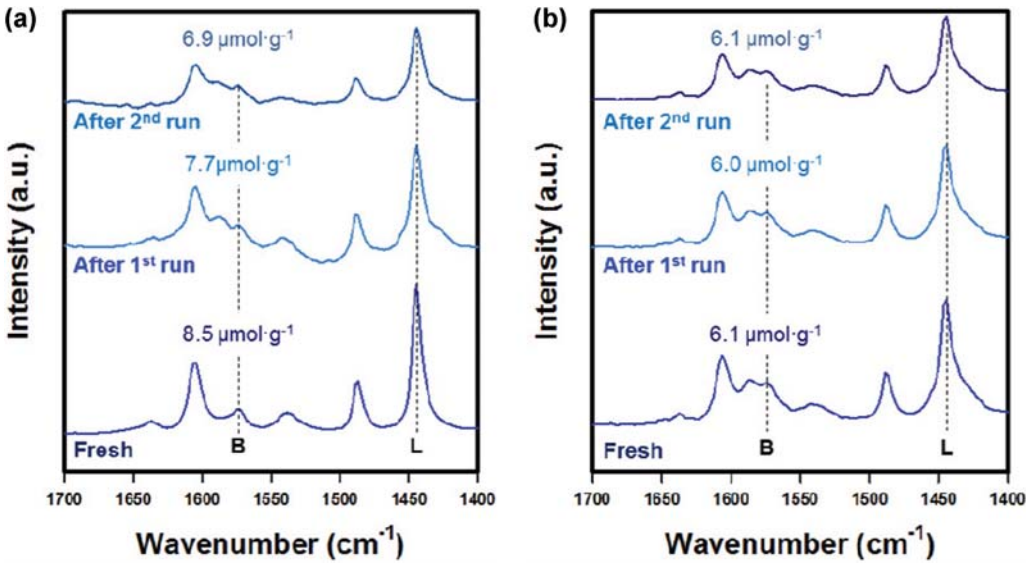

Fig. S1. Pyridine-chemisorbed FT-IR spectra of the as-prepared (a) $eHNb_3O_8$-C and (b) $eHNb_3O_8$-A samples. From bottom to top, the spectrum is for the fresh sample, for the spent sample after the first run, and for the spent sample after the second run, respectively.

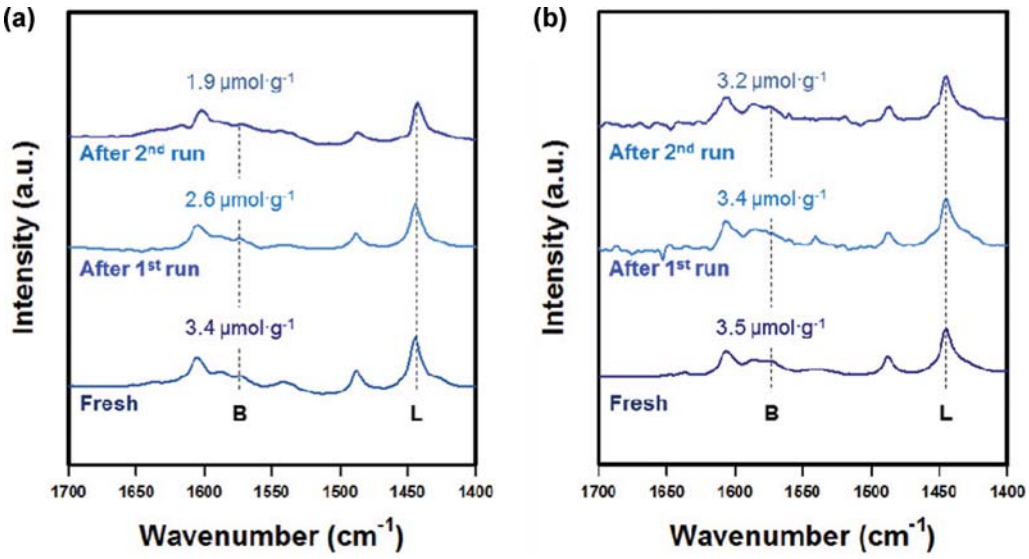

Fig. S2. Pyridine-chemisorbed FT-IR spectra of the 523 K-pretreated (a) $eHNb_3O_8$-C and (b) $eHNb_3O_8$-A samples. From bottom to top, the spectrum is for the fresh sample, for the spent sample after the first run, and for the spent sample after the second run, respectively.

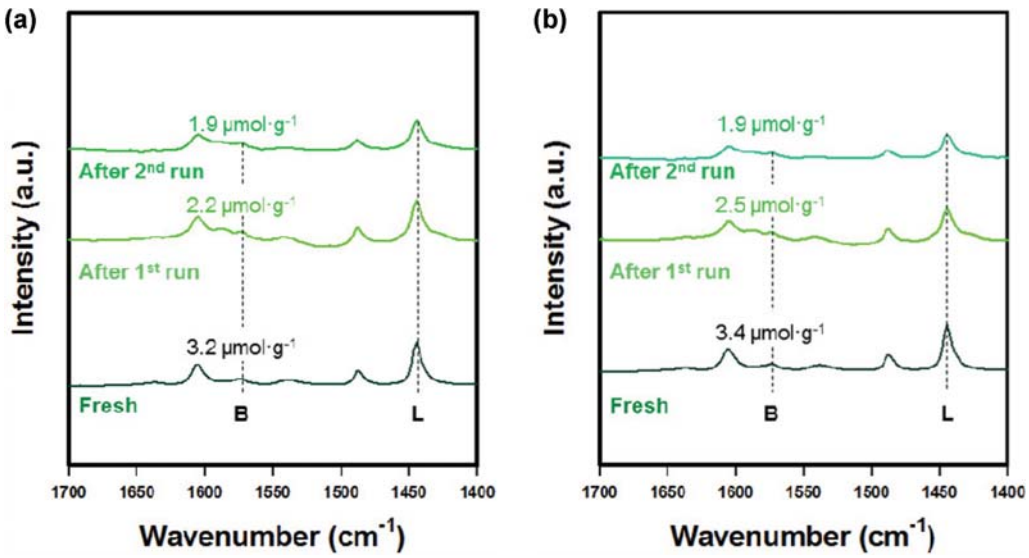

Fig. S3. Pyridine-chemisorbed FT-IR spectra of the 523 K-pretreated (a) $eHNb_3O_8$-A1 and (b) $eHNb_3O_8$-A2 samples. From bottom to top, the spectrum is for the fresh sample, for the spent sample after the first run, and for the spent sample after the second run, respectively.

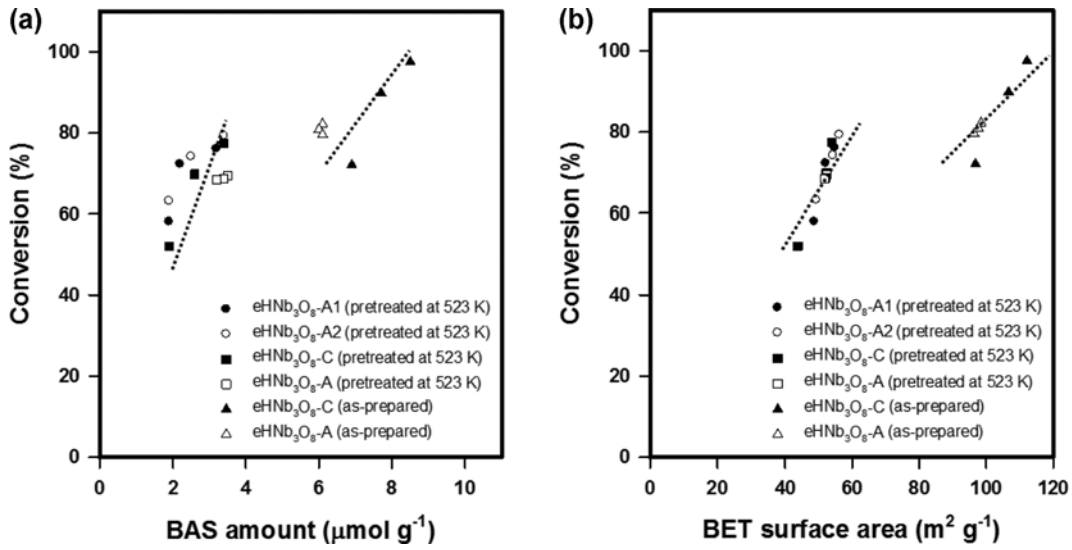

Fig. S4. Correlations of the activities and with (a) the BAS amount and (b) BET surface area of the fresh and spent catalysts samples tested in this work.

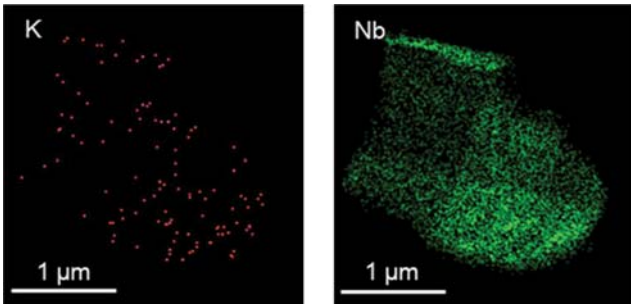

Fig. S5. K and Nb EDS mapping images of HNb_3O_8-A derived from the solid-state mixing.

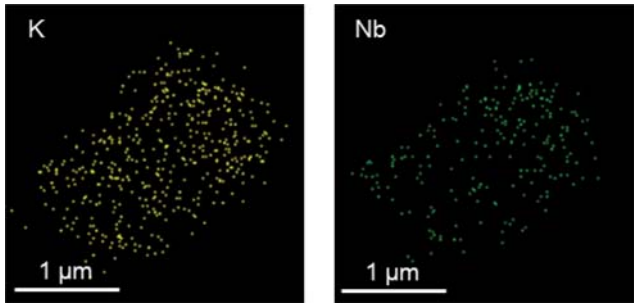

Fig. S6. K and Nb EDS mapping images of KNb_3O_8-A derived from the solid-state mixing.

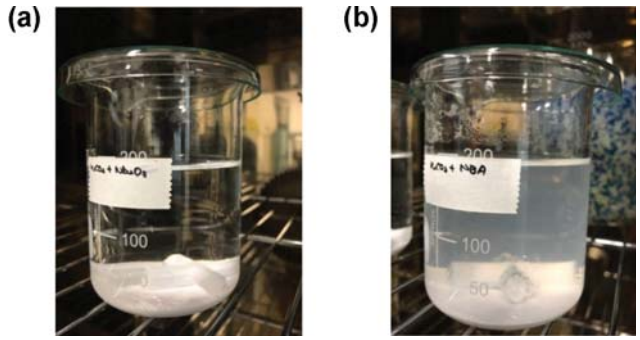

Fig. S7. Optical pictures of the beaker containing (a) Nb_2O_5 or (b) niobic acid (NBA) in an aqueous solution of K_2CO_3.